

Identification of Key Contributive Compounds in a Herbal Medicine: A Novel Mathematic—Biological Evaluation Approach

Cheng Zhang, Ning Wang, Yu Xu, Hor-Yue Tan, and Yibin Feng*

A pattern or syndrome in response to a multicomponent system is the actual target of herbal medicine treatment. However, it is a substantial challenge to fill the gap between a contributive compound profile in herbal medicine (especially a formula) and its biological features. This study aims to establish a feasible component-mining strategy, which provides a strong prediction of key compounds in support of experimental and clinical observations. Given interdisciplinary scope of life science and mathematical statistics, the relationship between chemical profile and bioactivities is measured by a model termed mathematical prediction bioactivity, in which gray relational analysis, multiple linear/non-linear regression analysis (including t-distributed stochastic neighbor embedding), and radial basis function analysis are involved. R language programming-dependent analysis is adopted with add-on packages, including UniDOE, Factoextra, FactoMineR, Factanal, Rtsne, and Nnet. By using this assessment method in a biological experiment, it is identified that 6-shogaol extracted from Ginger-Coptis formula (a herbal formula) is beneficial for diabetic retinopathy (DR) treatment. The study provides both a novel compound 6-shogalol for DR treatment and a new strategy for mining key contributors in a multicomponent system.

centuries, as a combination of several medicinal herbs, herbal formula has made eminent contributes to reverse pathological malfunctions.^[1,2] Meanwhile, in the past years, the U.S. FDA possesses positive attitude on approving medicinal herb-related clinical trials and application permission. For example, one of the renowned botanical drugs Kunecatechins, an extract from green tea leaves, have been approved by FDA in 2006 for treating external and perianal warts.^[3] Undoubtedly, conventional approaches have achieved certain success, but the drawbacks are conspicuous as the following four aspects: First, abundant fractionations and bioassays. Second, in vitro or in silico results may be irreproducible in animal and clinical study. Third, it undergoes a risk of neglecting the interactive actions of coexisting factors. Fourth, different compounds and combinations may be accountable for various specific diseases. Therefore, it is pressing to develop a technique that enables us to


1. Introduction

Regarding the rapid development in modern life science, experimental data are unprecedentedly complicated than ever before, which makes it difficult to capture the key feature of a multicomponent system. One of the well-known challenges in pharmaceutical science is understanding the therapeutic action of a herbal medicine formula by current approaches, especially in mining bioactive compounds for treating diseases. For

theoretically and efficiently understand the relative contribution of each component in a multicomponent system, which offers us a massive benefit for accelerating drug discovery. In contrast with conventional methods, modern technique performs a holistic view without predefined characteristics. The machine learning-dependent objective evaluation may have a beneficial impact on accurately predicting the core bioactive component.^[4] Additionally, HPLC-based chromatographic fingerprint analysis is prone to select as a sensitive and suitable technique to provide chemical profile.^[5] It enables us to calculate and elaborate the relevant contribution of each compound with its corresponding bioactivities. Thus, High Performance Liquid Chromatography concomitant with a novel compound-mining strategy were applied in this study.

Diabetic retinopathy (DR) is a vision-threatening disease characterized by retinal morphological and functional disorders. It remains the leading cause of blindness in working-age adults.^[6] Around 3.2 million people worldwide are suffering from DR.^[7] However, conventional anti-DR therapies, including laser photocoagulation and vitrectomy surgery, are unsatisfactory due to the unavoidable side-effects.^[8] Notably, medicinal herbal treatment exerted positive effects on alleviating DR-induced complications.^[9] Among these, Ginger-Coptis formula

C. Zhang, Dr. N. Wang, Dr. Y. Xu, Dr. H.-Y. Tan, Prof. Y. Feng
School of Chinese Medicine
LKS Faculty of Medicine, the University of Hong Kong
1/F, 10 Sassoon Road, Pokfulam, Hong Kong S.A.R., China
E-mail: yfeng@hku.hk

 The ORCID identification number(s) for the author(s) of this article can be found under <https://doi.org/10.1002/adts.202000279>

© 2021 The Authors. Advanced Theory and Simulations published by Wiley-VCH GmbH. This is an open access article under the terms of the Creative Commons Attribution-NonCommercial-NoDerivs License, which permits use and distribution in any medium, provided the original work is properly cited, the use is non-commercial and no modifications or adaptations are made.

DOI: 10.1002/adts.202000279

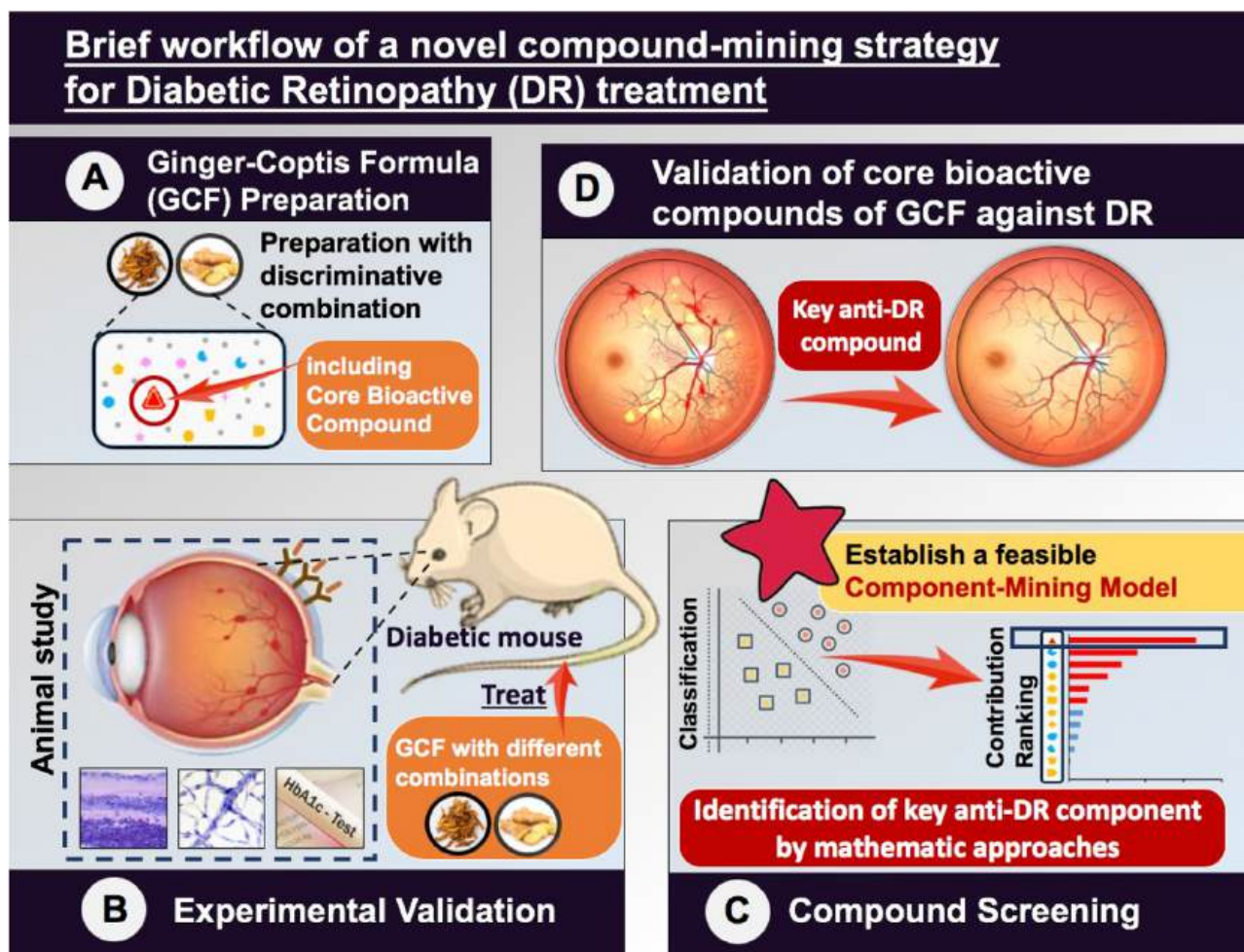


Figure 1. Brief schematic of establishing a novel compound-mining strategy in a multi-component system for the treatment of diabetic retinopathy.

(GCF), a mixture of herbal medicine *Zingiber Officinale* (ginger) and *Coptidis Rhizoma* (coptis), is a promising candidate for DR management, which has long-term engaged in treating numerous endocrine diseases in Chinese medicine.^[10] More specifically, ginger consumption was reported to improve the glycemic status and lipid profile.^[11,12] Whereas, coptis was documented to ameliorate dysfunction of lipid metabolism and glycometabolism.^[13,14] In our study, it is the first attempt to identify the core anti-DR bioactive components in GCF by a model termed Mathematical Prediction-Bioactivity (Figure 1).

2. Results

2.1. Ginger-Coptis Formula Suppressed Retinal Microvascular Complications in Diabetic Mice via Hypoglycemia-Independent Manner

To explore whether Ginger-Coptis formula (GCF) and its bioactive compounds possesses anti-DR effect, animal experiment has conducted for the preliminary verification of drug efficacy. As shown in Figure 2A, type I diabetic mouse was established by the injection of STZ (55 mg/kg) for consecutive 5 days. Those

mice with fasting blood glucose ranging from 15 to 22 mmol L⁻¹ were considered as successfully established model and treated with various interventions. Apart from the normal and model group, mice have also undertaken an 8-week treatment with insulin (2 U/kg/d), ginger extract (20 mg/kg/d), Coptis extract (20 mg/kg/d), and GCF (1:1, total 20 mg/kg/d), respectively ($n = 5/\text{group}$). Retinal microvascular complications are the leading pathological changes for DR progression, including microvascular remodeling and hyperpermeability. Therefore, the assessment of retinal vasculature was conducted, including the detection of blood-retina barrier (BRB) permeability using Evans blue dye for quantitation. It was manifested that Type I diabetic mice with all 3 treatments, including ginger, coptis, and GCF (1:1), had the inhibitory effect on the increasing acellular vessels, proportion of endotheliocytes and pericytes (E/P ratio), and BRB breakdown, but insulin insignificantly prevented the leakage of Evans blue in retina (Figure 2B–E) ($p > 0.05$ vs model). Meanwhile, the anti-hyperglycemic action among groups were measured as well (Figure 2F,G). Type I diabetic mice treated with insulin, ginger, coptis, or GCF (1:1) significantly ameliorated the hyperglycemia ($p < 0.05$ vs model) as evidenced by the reduced fasting blood glucose and serum HbA1c (an indicator for general

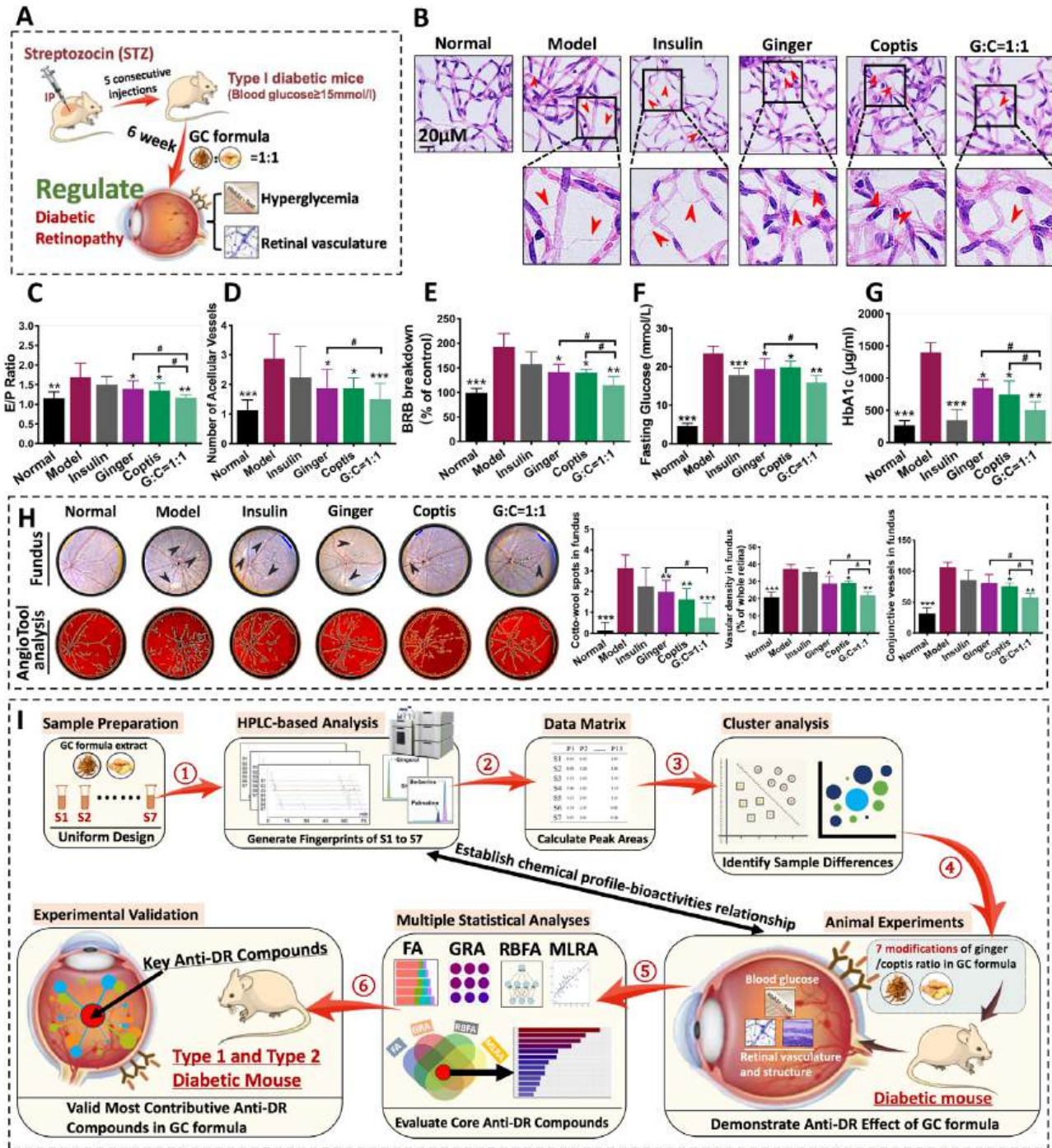


Figure 2. Ginger-Coptis formula (GCF) inhibited retinal vasculopathy in Type I diabetic mice and construction of “mathematical prediction-bioactivity” model. A) Diagram of preliminary experiments for measuring the potential anti-DR effect of GCF. B) Representative figures of H&E-stained retinal vascular isolation. Acellular capillary are pointed with white arrow. Oval-like cells located within vessels are endothelial cells, whereas cells lying on the capillary walls are pericytes. C,D) Quantification of E/P ratio (endothelial cells/pericytes) and acellular capillaries. E) Blood-retina barrier breakdown as percentage of model group assessed by Evans blue. F,G) Detection of 8-week fasting blood glucose and HbA1c in STZ-induced diabetic mice. H) Fundus photography captured by a 78D ophthalmoscope (left panel). AngioTool is utilized to quantify the cotton-wools pots (pointed with black arrow), vascular density, and conjunctive vessels in the retinal fundus. I) Experimental design for the identification of core anti-DR compound in GCFs (7 modifications) by “mathematical prediction-bioactivity” model. Insulin: 2 U/kg/d; Ginger or Coptis extraction: 20 mg/kg/d; G:C = 1:1: 20mg (G+C)/kg/d. All data are presented as mean ± SD based on five independent experiments. * $p < 0.05$, ** $p < 0.01$ and *** $p < 0.001$ versus Model.

Table 1. Peak areas of 13 compounds in GCF.

	P1	P2	P3	P4	P5	P6	P7	P8	P9	P10	P11	P12	P13
S1	0.362	0.522	1.809	0.420	0.859	1.649	0.775	3.816	3.925	15.482	1.302	14.413	1.073
S2	0.983	1.258	4.275	0.975	1.985	3.868	1.751	9.241	9.697	39.762	2.510	13.579	1.849
S3	1.190	1.630	5.295	1.151	2.379	4.843	2.240	11.652	11.665	49.378	2.488	11.804	1.589
S4	1.064	1.619	5.696	1.283	2.788	5.399	2.448	13.582	13.195	57.146	1.207	9.804	1.186
S5	1.517	2.006	7.052	1.634	4.671	8.838	4.435	17.544	16.341	69.515	1.183	8.501	1.213
S6	1.737	2.310	8.202	1.978	5.611	10.693	5.335	21.391	19.059	81.130	1.015	5.286	0.812
S7	1.968	2.608	9.222	2.142	6.426	12.129	5.663	22.507	21.245	93.282	0.833	3.899	0.457

gauge of blood glucose and diabetic complications). However, the hypoglycemic action of GCF (1:1) was lower than insulin. More strikingly, the inhibition of retinal vascular lesion by GCF (1:1) was superior to that of ginger or coptis extract alone. Consistently, the significant decrease of retinal vascular density and conjunctive vessels were demonstrated in Type I diabetic mice treated with ginger, coptis extraction, and GCF (1:1) respectively, which is analyzed by fundus photography with *AngioTool* (Figure 2H). In addition, the cotton-wool spots in retinal has been quantified by fundus photography with *ImageJ*, which was located in the nerve fibre layer as a discoloration representing retinal vascular infarction, ischemia, and accumulations of axoplasmic material in the nerve fiber layer. It was illustrated that Type I diabetic mice intervened with ginger, coptis, and GCF (1:1) led to the dramatic reduction of cotton-wool spots ($p < 0.05$ vs model), but inconspicuous in that of insulin intervention ($p > 0.05$ vs model). Significant differences were observed between control and model group for all glycemic and vascular assays in this part. Collectively, 3 conclusions can be drawn from these data. First, the insulin-like significant hypoglycemic effect is insufficient to postpone DR progression. Second, GCF (1:1) exhibited more effective action on suppressing retinal vascular degeneration and hyperglycemia than that by ginger or coptis extraction. Third, the action of anti-DR compounds in GCF (1:1) is independent of glycemic control. Prompt by these observations, a specific workflow was designed to identify the core anti-DR bioactive compound in GCF, including statistical models (Figure 2I), aiming to clarify the relationship between HPLC fingerprints of GCFs and its related pharmacological activities followed by screening out the bioactive anti-DR compounds in GCF.

2.2. Uniform Design-Based Dose Optimization of GCFs and HPLC Fingerprints Analysis

Uniform design (UD) was applied to modify the GCF with a series of combinations of ginger and coptis, aiming to lay a foundation for disclosing the spectrum of pharmacological effects of GCF for DR treatment. Taken advantage of quasi-Monte Carlo and number-theoretic methods, uniform design was adopted to design a two-factor and seven-level $U_7(7^2)$ experiment. As shown in **Figure 3A** the representative ratios of ginger/coptis in GCF was uniformly scattered into seven combinations. The total weight of ginger and coptis extracts was constant in each level.

In the HPLC-related fingerprints analysis, 13 common compounds existed in 7 modified GCF were discerned by a gradient

elution procedure (Figure 3B, **Table 1**), in which palmatine, berberine, and 6-gingerol were the principal ingredients and highlighted in the enlarged images in Figure 3B. The peak areas of 13 compounds were used as independent variables for further statistical analyses. Unsupervised learning approaches including k-means-based PCA, cluster analysis, and t-distributed stochastic neighbor embedding could interpret the discrimination or interrelationships among modified GCF, which were achieved by minimizing the within-cluster variances or linearly/non-linearly mapping the dataset in a low-dimensional representation respectively (Figure 3C). Based on Figure 3B,C, 13 selected fingerprints are primarily recognized into 3 categories with different compositions. These findings suggested that there are distinctions in chemical profiles among 7 combinations, which could be adopted for subsequent pharmacological experiments.

2.3. Diversified Characteristic of GCFs on Glycemic Control

To comprehensively disclose the relationship between biological activities and UD-based GCF modifications (S1–S7), a series of DR-related assays were conducted. The parameters of pharmacological assays consisted of 3 aspects, including blood glucose monitoring, retinal vasculature, and retinal morphology (especially the retinal nerve). For glycemic control, besides the normal control group, insulin group (2 U/kg/d), and model group (STZ-induced Type I diabetic mice without treatment), other mice have gone through particular 8-week treatments as follows (20 mg/kg in total per day in each group): ginger or coptis extract, S1 (ginger:coptis (G:C) = 12.9:1), S2 (G:C = 3.6:1), S3 (G:C = 1.8:1), S4 (G:C = 1:1), S5 (G:C = 1:1.8), S6 (G:C = 1:3.6), S7 (G:C = 1:12.9). As shown in the body weight measurement, the normal mice was heavier than model mice ($p < 0.05$ vs model), but insignificant when compared with other groups ($p > 0.05$ vs model), suggesting the treatments with insulin, ginger or coptis alone, or GCFs (S1–S7) were not sufficiently effective to reverse the diabetes-induced weight loss (Figure 3D). For the investigation of hyperglycemia management among groups, the blood glucose-related biological parameters were detected, including fasting blood glucose (FBG), HbA1c, and intraperitoneal glucose tolerance test (IPGTT). Insulin significantly lowered the mice blood glucose ($p < 0.001$ vs model). Although the anti-hyperglycemia effects of several intervention were not as remarkable as insulin, the treatments of ginger, coptis extract, or GCFs (S3, S4, S5, S6, and S7) possess hypoglycemic action in terms of results from FBG, HbA1c, and IPGTT ($p < 0.05$ vs model) (Figure 3E–H). In

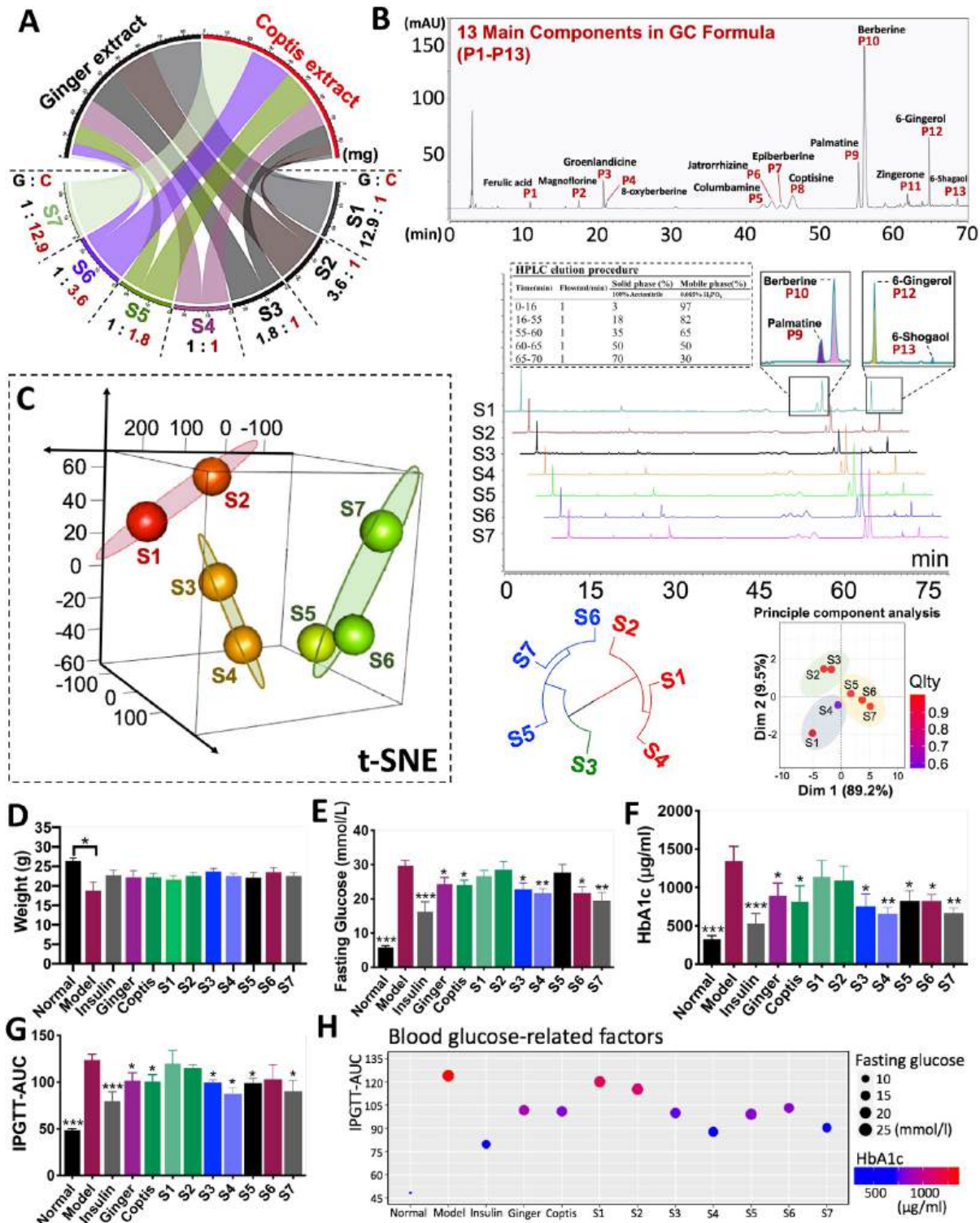


Figure 3. Uniform design-based dose optimization of GCFs led to diversified characteristic of glycemic control. A) Preparation of GCFs (7 modifications) by Uniform Design. B) Chromatographic fingerprints of GCFs with a gradient elution procedure. P1–P13 are marked in the fingerprint. K-means-based cluster analysis and PCA are shown below. C) t-SNE (t-distributed stochastic neighbor embedding) plot represents three differentially grouped GCFs. D) Changes of body weight in 8-week normal control or diabetic mice with various treatments, including insulin (2 U/kg/d); ginger or coptis extraction (20 mg/kg/d); and GCFs (S1–S7, the abbreviation “S” stands for sample, 20 mg (G+C)/kg/d). E, F) Detection of 8-week fasting blood glucose and Serum HbA1c. G) Quantification of Areas Under the Curve (AUC) by intraperitoneal glucose tolerance test (IPGTT). H) Scatterplot of the blood glucose-related factors in each group. All data are presented as mean \pm SD of five independent experiments. * p < 0.05, ** p < 0.01 and *** p < 0.001 versus Model.

conclusion, the interventions of ginger, coptis extract, or GCFs (S3, S4, S5, S6, and S7) were capable of controlling blood glucose in DR progression. Furthermore, specific modified GCF was more effective than ginger or coptis extraction alone. Finally, based on uniform design, GCFs with 7 modified samples (S1–S7) could lead to different biological activities in diabetic mice, which laid a foundation of finding out the core anti-DR compounds in GCFs. Further experiments on the GCFs-related modulation of retinal morphology and vasculature in diabetic mice have been measured.

2.4. Suppression of DR-induced Retinal Vasculopathy and Neuropathy by GCFs

To further address whether GCFs (S1–S7) ameliorate retinal vasculopathy in Type I diabetic mice, a series of experimental validations have been carried out, including fundus photography, vessels isolation, BRB permeability, and vasculature immunofluorescence in whole-mount retina. More specifically, in the fundus photography, significant decrease of vascular density and conjunctive vessels were demonstrated after the treatments of coptis, S3, S4, and S7, contributing to the reversion of DR damage ($p < 0.05$ vs model) (Figure 4A–D). Moreover, the hyperpermeability of BRB were improved by ginger, Coptis, and S3–S7 treatments, which is measured by Evans blue leakage in the retina ($p < 0.05$ vs model) (Figure 4E). Further trypsin-based retinal vasculature digestion was performed to evidence the effect of GCFs on retinal neovascularization. The quantitation of E/P ratio was declined when DR mice treated with ginger, coptis, S1, S3, S4, S7 ($p < 0.05$ vs model), while the decrease of acellular capillaries was significant in groups of coptis, S2–S4, S6, S7 ($p < 0.05$ vs model) (Figure 4F–H). To in-depth understand the morphological features of DR-related retinal neovascular area, the visualization of whole-mount retina was performed by immunofluorescence. The production of retinal microaneurysms in diabetic mice was suppressed by ginger, coptis, S3, S4, and S7 intervention ($p < 0.05$ vs model). Meanwhile, the increase of vascular density was restrained by ginger, coptis, S2–S5, and S7 treatments. DR-driven sprouting conjunctive vessels in retina was attenuated by ginger, coptis, S3–S4, and S7 treatments (Figure 4I). Additionally, in terms of vascular abnormalities, there was significant difference between the normal control and model group ($p < 0.05$ vs model), but it is insignificant when the model was compared with insulin treatment ($p > 0.05$ vs model). Taken together, these data suggested that insulin-induced hypoglycemia cannot effectively suppress the DR-related vascular pathological alterations like ginger, coptis or GCFs.

Retinal neurodegeneration is a pathological process concurrently occurred with vasculature abnormalities in DR, resulting in the irreversible reduction of retinal neurons and thickness of inner retinal layers. Hereby, the biological parameters of morphological structure of retina after various treatments in DR progression has been measured. It was shown that a decrease of retinal neurocytes, including retinal ganglion cells (RGCs) and amacrine cells (ACs), has been detected when DR mice treated with ginger, S1–S3, S5 ($p < 0.05$ vs model). However, ginger, coptis, and GCFs were incapable of postponing the reduction of thickness of inner retinal layers, including inner plexiform layer

and inner nuclear layer ($p > 0.05$ vs model) (Figure 4J). Similar to the anti-angiogenic effect, the retinal neuropathy is not existed in normal control group than that in model group ($p < 0.05$ vs model), however, insignificant impact was in the comparison between insulin and model group ($p > 0.05$ vs model). These data suggested that ginger extract, S1–S3, and S5 had a potent effect on the maintenance of integrity of retinal neurons, but failed to inhibit the thinning of inner retinal layers. However, insulin is insufficient in the deceleration of retinal vasculopathy and neuropathy. The potential relevance between HPLC-based chemical profile and bioactivities will be further analyzed by numerous mathematical methodologies.

2.5. Predictive Identification of Pivotal Anti-DR Compounds in GCFs by Multivariate Statistical Models

The information of GCFs-related experimental validation for DR treatments was assessed by a combination of a series of statistical models, including factor analysis, gray relational analysis, radial basis function, and multiple-linear analysis. Afterward, the most contributive anti-DR compound derived from GCFs will be mathematically identified.

For the factor analysis (FA), it is suitable for simplifying the complex variables into fewer groups, aiming to reveal the common dimensions of factors and FA-based weight distribution.^[15] A number of factors (biological parameters) have decreased in terms of both factor score (weight of each factor) in a rotation matrix and its corresponding clinical meaning. As a result of this, 11 mutually independent factors were finally extracted from 14 pharmacological factors (Figure 5A). In particular, results of fundus photography and random blood glucose were eliminated in the data matrix, since the loading value of these two indices were approximately equal to at least 2 factors. Fewer quantity of factors was beneficial for the improvement of interpretative degree for data variability. In terms of the rotation sums of cumulative squared loadings, the remaining 11 intercorrelated factors could represent 83.4% of the original data information. On the basis of factor score and clinical significance, 11 factors reflected 3 enriched factors, which represented 3 aspects of DR-related biological features, including glycemic control (factor 1), retinal vasculature (factor 2), and retinal neuromorphology (factor 3). In Figure 5A, the sub-indicators affiliated to each enrichment factor were shown as the follows: F1 (HbA1c, fasting glucose, IPGTT), F2 (blood-retina barrier, acellular vascular, E/P ratio, vessel density in whole-mount retina, conjunctive vessels in whole-mount retina), and F3 (thickness of inner nuclear and plexiform layer, number of retinal neurons in RGC layer).

For the gray relational analysis (GRA), it is a mathematic approach to solve the multi-attribute and decision-making problem in a complex relationship, which involved multiple factors and variables.^[16] Taking the biological parameters of enriched factor 1–3 as the reference sequence and 13 compounds of GCFs as the independent variable sequence, we calculated the gray relational grade (GRG) of the compounds in each factor by GRA. GRG represented the efficiency contribution of each ingredient for the DR treatment (Figure 5B). As shown in the results, compound P1 (Peak 1), P11, and P13 had a higher correlation with F1, all of which are greater than 0.7. This outcome indicated that these

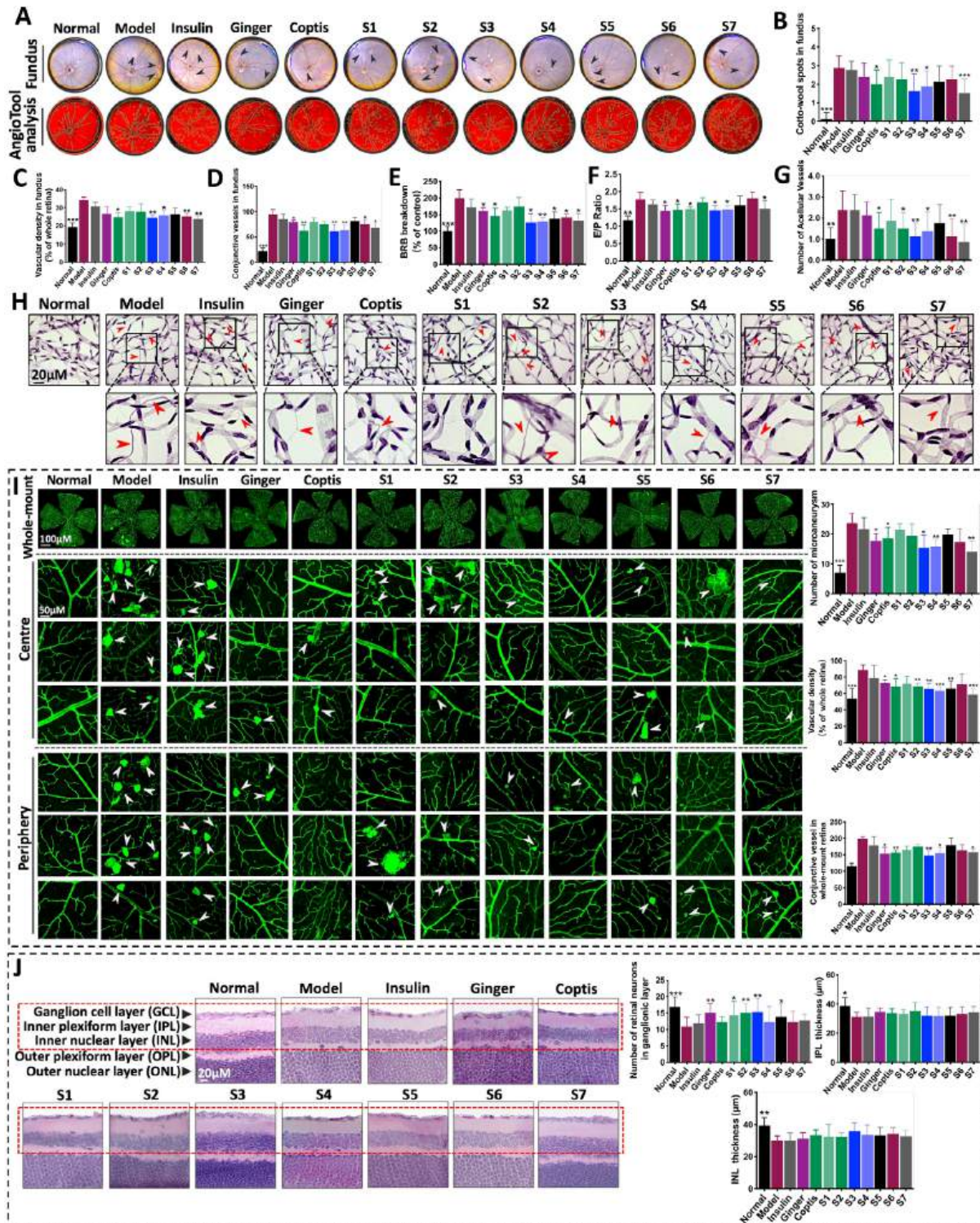


Figure 4. Inhibition of DR-induced retinal vasculopathy and neuropathy through GCFs treatments. A,B) Ophthalmoscope-based fundus photography. Cotto-wool spots are quantified and figured out with black arrows. C,D) Quantification of vascular density and conjunctive vessels in retina by funds photography. E) Assessment of BRB permeability by Evans blue assay. F-H) Retinal trypsin digestion assay for measuring E/P ratio (endothelial cells/pericytes) and acellular capillaries. I) Visualization of whole-mount retina by immunofluorescence (isolectin GS-IB4). Retinal microaneurysms are pointed with white arrows (left panel). AngioTool-dependent quantification of microaneurysm, vascular density, and conjunctive vessels are shown in the right panel. J) Representative figures of retinal tissue sections by H&E staining (left panel). The quantification of retinal neurons in RGC layer are shown in the right panel, including retinal ganglion cells and amacrine cells. All data are indicated as mean \pm SD of five independent experiments. * p < 0.05, ** p < 0.01 and *** p < 0.001 versus Model.

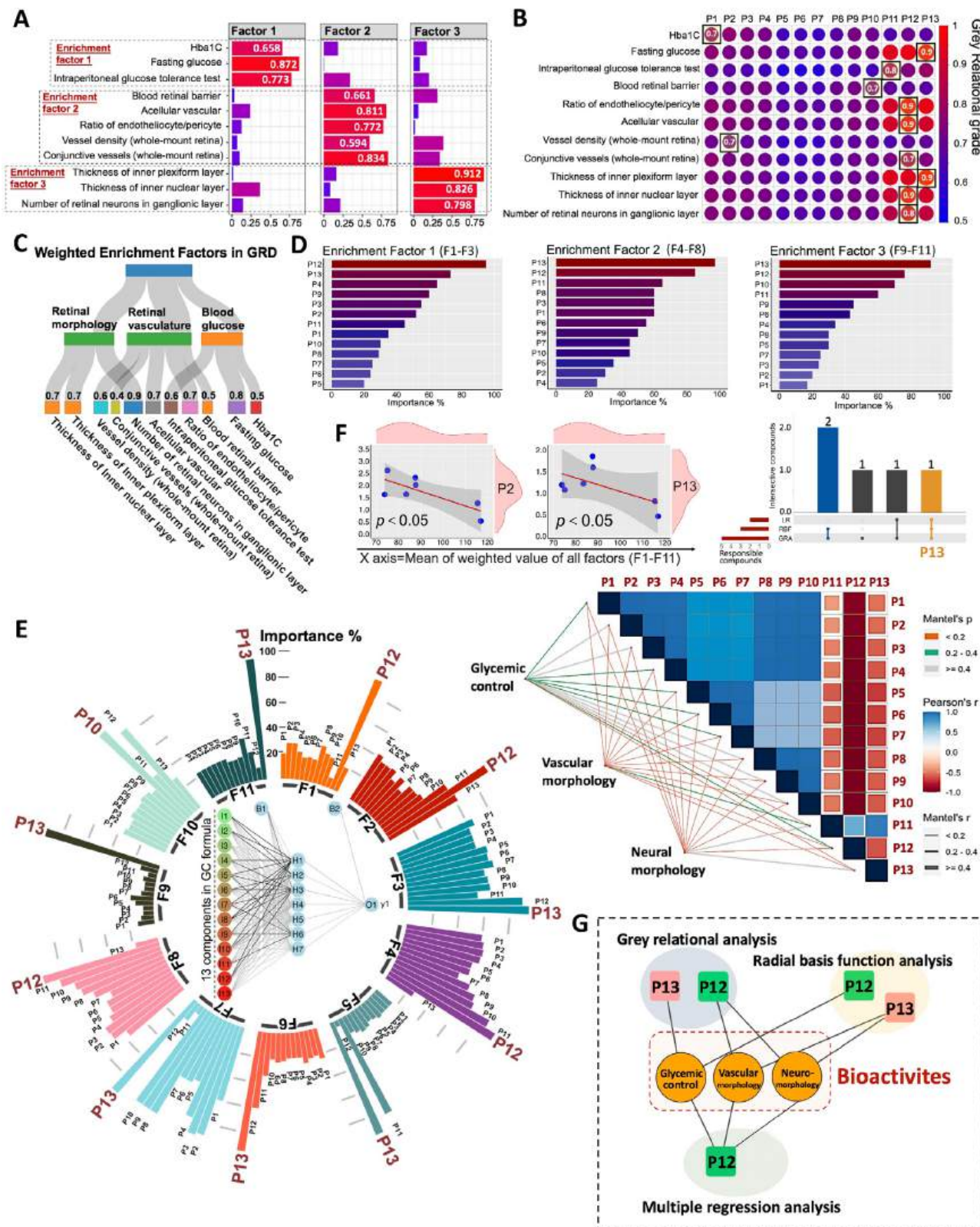


Figure 5. Predictive identification of core anti-DR ingredients in GCFs by mathematical prediction-bioactivity model. A) Result of factor analysis indicates the 11 DR-related biological parameters in 3 factors. The factor loadings (factor score) of each sub-item are shown in the panels. Longer bar corresponds to stronger weight of the indices to its related factor. B) Gray relational grade of the relationship between 13 compounds (P1-P13) in GCFs and 11 biological factors, which is analyzed by gray relational analysis. Larger value indicates the stronger correlation. C) Recalculation of gray relational grade by

3 peaks were strongly associated with glycemic control. In addition, compound P2, P10, and P12 had closer correlation with F2 as the GRG larger than 0.7, suggesting that these 3 ingredients played a vital role in reversing DR-induced retinal vasculopathy. Meanwhile, compound P12 and P13 were closely related to F3 with the GRG larger than 0.8, indicating that these two ingredients possessed profound pharmacodynamics on the suppression of retinal neuropathy in DR progression. To further discriminate the most contributive compound in each enriched factor (F1–F3), data enrichment has been conducted by imposing the factor score (FS) as a coefficient on the calculation of modified GRG (factor score IGRG) in GRA model. Then, a recalculated GRG was obtained in each sub-indicator as shown in the Sankey diagram (Figure 5C). The results suggested that P13 in term of fasting glucose (GRG = 0.8) had a significant contribution for regulating blood glucose (F1). while, P12 in both terms of E/P ratio (GRG = 0.8) and acellular vascular (GRG = 0.8) had dominant position in the improvement of DR-caused retinal vasculopathy (F2). Also, P13 in term of number of retinal neurons in ganglionic layer possessed a large weight value (GRG = 0.9) in the abolishment of DR-related retinal neuropathy. Based on these findings, both P12 and P13 were mathematically predominant for the suppression of retinal vascular and neural abnormalities in DR progression.

For radial basis function (RBF) analysis, it provides a more sophisticated decision boundary for classifying multiple clusters by radian basis transformation function, including non-linear neural network training, weighting vectors and linear separation.^[17] Thus, it describes the liner and non-liner interaction between the values of input and output by an artificial neural network. A final probabilistic value (RBF score) was obtained for predicting the contributive weight of 13 compound in response to 11 factors (Figure 5D,E). The larger the RBF score is, the higher the contributive degree is. According to RBF analysis, P12 and P13 coincidentally indicated much greater association with F1 (glycemic control) and F2 (reversal of retinal vasculopathy), suggesting the desirable prevention of hyperglycemia and retinal vascular lesions. In addition, P10, P12, and P13 had substantial impact on the improvement of retinal neuropathy (F3). These data suggested that both P12 and P13 are defined as the most weighted anti-DR compounds, which were consistent with the outcome of GRA.

For multiple linear regression analysis (MLRA), linear regression is adopted to explain the interaction between one continuous response variable and two or more explanatory variables.^[18] All factors were considered as the response variable, while the peak areas of 13 compounds were regarded as the explanatory variables. Linear regression model has been established when *p*-value is less than 0.05. The intensity of relevance between the bio-

logical efficacy and compounds has been evaluated by the value of regression coefficient (Figure 5F). As a result of MLRA, only P2 and P13 was filtered into equation (linear regression *p* < 0.05). Among these, P13 is the only mutual component identified by GRA, RBF, and MLRA as shown in the bar plot (Figure 5F). These findings indicated that P13 may consider as a key contributor for DR management.

In summary, multiple mathematic models with HPLC fingerprints have achieved promising prediction for enhancing the understanding of core contributive compounds, especially the P12 and P13. Hereby, as shown in Figure 5G, it is indispensable to carry out pharmacological experiments for further confirming the anti-DR effect of both P12(6-gingerol) and P13(6-shogaol), which were discerned as high-weighted compounds in GCFs accountable for DR treatment.

2.6. 6-Shogaol Was Verified as the Most Contributive Compound in GCFs for DR Treatments (Type I and Type II Diabetes)

Based on the multivariate model predictions, both P12 (6-gingerol) and P13 (6-shogaol) were potentially identified as the most weighed ingredients against DR. Therefore, experimental validation was carried out for testing the accuracy of mathematical models. Apart from STZ-induced Type I diabetic mouse, leptin receptor-deficient Type II diabetic model (db/db mouse) was included for comprehensive diabetes study. Notably, PCA analysis for the composition of herbal combinations indicated that S4 is the mean-centering point in two dimensions (Figure 3B, showing a central position among other points (S1–S3, S5–S7). Combined with its potent anti-DR effect with its mean-centering merit, S4 (ginger: coptis = 1:1) was further used to treat both Type I and Type II diabetic mice as a GCF reference. Similar as before, the management of DR was determined by 3 aspects, including glycemic control, retinal vasculopathy, and neuropathy. It was showed that there were insignificant changes of body weight between the treatment of S4 versus 6-gingerol (20 mg/kg) or 6-shogaol (20 mg/kg) in both Type I and Type II diabetic mice (*p* > 0.05 vs Type I model; *p* > 0.05 vs Type II control). For glycemic control, the value of fasting blood glucose, HbA1c, and the Area Under Curve (AUC) of IPGTT was decreased by 6-gingerol or 6-shogaol treatment. However, insulin has much better hypoglycemic effect than S4, 6-gingerol or 6-shogaol (Figure 6A).

To assess the DR-induced damage of retinal vasculature, both fundus photography and H&E- or immunofluorescence-dependent retinal vascular visualization were performed. There was a significant downward trend in the following biological parameters, including the quantity of cotto-wool spots, conjunctive vessels, vascular density, E/P ratio, and acellular vessels, when diabetic mice were treated with 6-gingerol or 6-shogaol (*p* < 0.05

imposing factor score as a coefficient to GRG (factor score IGRG) in the model of gray rational analysis. D,E) Results of radial basis function analysis, the probabilistic value shown in the barcharts indicated the contributive degree of compounds in each enrichment factor. A RBF neural network is located in the center of circular histogram, which shows the weight changes of 13 compounds with training iterations by a neural interpretation model. The wider line width indicates the greater magnitude of weight. F1-HbA1c; F2-Fasting glucose; F3-IPGTT-AUC; F4- integrity of blood-retina barrier; F5- E/P ratio; F6-Acellular vascular; F7- Conjunctive vessels (whole-mount retina); F8-Vessel density (whole-mount retina); F9-Number of retinal neurons in retinal ganglion cell layer; F10-Thickness of inner plexiform layer; F11-Thickness of inner nuclear layer; F) Pairwise comparisons (Mantel and Pearson test) and multiple linear regression results of all factors (F1–F11) and corresponding bioactivities. The linear regression model is established when *p* < 0.05. G) The network profile illustrates the predicted high-weighted compounds for DR treatment, including the regulation of blood glucose, retinal vasculature, and neuromorphology.

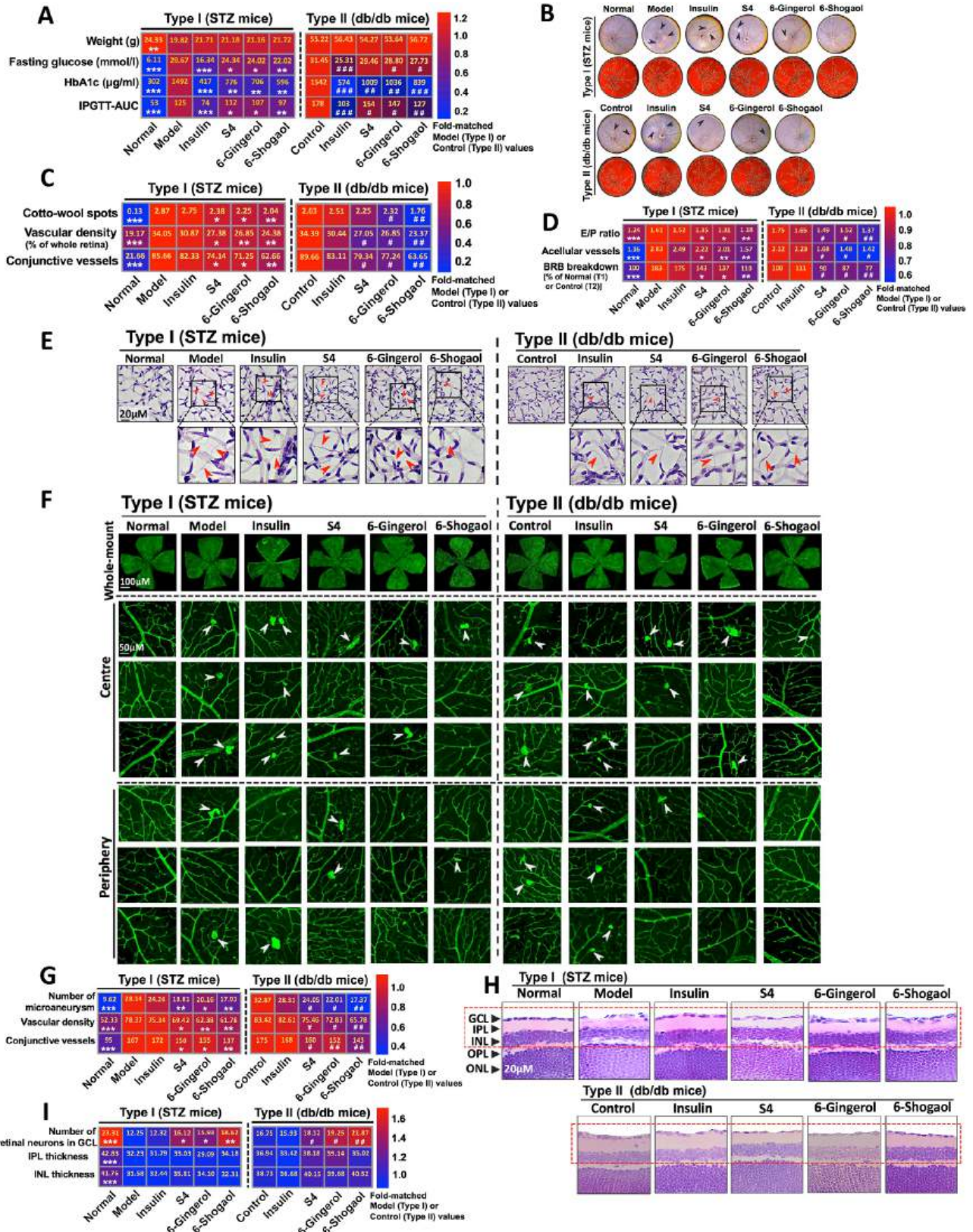


Figure 6. 6-shogaol is demonstrated as the most contributive ingredient in GCFs for DR treatment in both Type I and Type II diabetic mice. A) Changes of weight, fasting glucose, HbA1c, an IPGTT-related AUC in both 8-week Type I (STZ intervention) and Type II (db/db) diabetic mice. B) Representative figures of fundus photography, Cotto-wool spots are pointed out with black arrows. C) Quantification of Cotto-wool spots, vascular density, and conjunc-

vs Type I model; $p < 0.05$ vs Type II control). These results were consistent in measuring the integrity of blood-retina barrier by Evan blue assay, while 6-shogaol is far superior to 6-gingerol or S4 for inhibiting DR-caused retinal vascular injury. Furthermore, after Type I and Type II diabetic mice treated with 6-gingerol and 6-shogaol, the production of retinal microaneurysm was reduced in whole-mount retina, suggesting the repression of retinal capillary pressure ($p < 0.05$ vs Type I model; $p < 0.05$ vs Type II control) (Figure 6B–G).

For DR-caused retinal neuropathy, in both Type I and II diabetic mice, S4 and its compounds (6-gingerol and 6-shogaol) inhibited the progressive loss of retinal neurons in RGC layer ($p < 0.05$ vs Type I model; $p < 0.05$ vs Type II control), in which 6-shogaol had more potent action than 6-gingerol and S4. However, the thinning of inner retinal layers (IPL and INL) was insignificantly alleviated via S4, 6-gingerol, and 6-shogaol treatments ($p > 0.05$ vs Type I model; $p > 0.05$ vs Type II control). Consistently, insulin is ineffective in inhibiting the degenerative changes of retinal microvasculature and neurons in diabetic mice (Figure 6H,I). Taken together, based on the mathematical analyses and experimental validation, 6-shogaol was evidenced as the most contributive ingredient in GCF for DR treatment. The model of “mathematical prediction-bioactivity” was a feasible way for screening bioactive compounds from multicomponent system (Figure 7).

3. Conclusion

In the conventional approaches, evaluation for pharmacological effect of herbal medicine mainly focuses on measuring abundant single compounds individually.^[19] Although such a strategy has achieved successes in the discovery of medicinal substances, there remains some room for improvement. Conventional methods may be time-consuming and expensive to repetitively analyze large-scale sample by typical approach. Also, it takes a risk of underestimating or overestimating of a single ingredient due to the coexisting effect of bioactive ingredients in a formula. Furthermore, even if the analytical process contains statistical methods like PCA and cluster analysis, it has a potential risk for inadequately reflecting the contribution of each coexisting ingredients in a formula. Each statistical approach is characterized by its own methodological merit and application scope. For example, logistic regression has been widely used in linearly modeling the mathematic relationship between two discrete outcomes (e.g., diseased or not diseased).^[20] However, it has two conspicuous defects, including the poor parameter estimation and ineffectiveness in certain interaction models (e.g., epistatic model). Herein, it is a challenge to establish a method that can make up the interactive shortcomings, while provide informative and sound theoretical basis for interpreting the contribution of multicomponent.

In this study, we established a model to figure out contributive bioactive compounds from a multicomponent system in a feasible way. A herbal formula-related biological experiments was applied to examine the feasibility of the proposed model. We, first of all, screened out anti-DR contributive compounds in GCF by a model termed mathematical prediction-bioactivity. It enabled us to theoretically and experimentally calculate the weight of compounds from a crude herbal medicine with its biological behaviors in a high-efficient manner. The advantages and disadvantages among statistical methods have been complementary. Based on Quasi-Monte Carlo method, uniform design is used to choose the most representative points in the experiment domain. An advantage of uniform design is the relatively less number of required assays to spread the design points to experimental domains.^[21] It is robust with the absence of preliminary strong assumption and obtains as much information as possible with fewer experiments than that of orthogonal design. GCF has been modified into 7 combinations (S1–S7) with uniformly distributed ratio of ginger and coptis. Discriminative constitution of multicomponent in GCF made the bioactivity evaluation of each compound for DR treatment more predictive. Based on uniform design, the composition profiles of herbal compounds in a crude herbal medicine was constructed by HPLC. It is sensitive to simultaneously separate a wide range of peaks of pure compounds prior to bioactivity detection. 13 compounds were drawn from GCF for further calculating its pharmacological contribution for DR therapy by using the model of mathematical prediction-bioactivity. Combined with the DR-related experimental data in the diabetic mice with various interventions, the results of factor analysis provide the biological evidence into 3 enriched factors (11 sub-items), including glycemic control (factor 1), retinal vasculature (factor 2), and retinal neuromorphology (factor 3), which is ideal to holistically measure the anti-DR effect of the core compound in GCF. With the combined analysis of gray relational analysis (GRA) and multiple linear regression analysis (MLRA), the association degree between GCF-derived compounds and bioactivities are presented, showing that 6-gingerol and 6-shogaol are responsible for the anti-DR action of GCF, in which retinal microvascular complications and neuroretinal degeneration are significantly improved. However, non-linearly separable problems can generate in both the GRA and MLRA calculation.^[22] Notably, radial basis function analysis (RBFA) is capable of transforming samples values into a high-dimensional descriptor space and then linearly calculated the contributive degree in a low dimensional space by a curve fitting method, also known as the artificial neural network.^[23] Since the non-linearly separable problem can be solvable by processing data in a high-dimensional computing environment. RBFA was incorporated in our compound-mining model with the merit of training the non-linearly separable variables into linearly separable dataset. In addition, multicollinearity problems are simultaneously

tive vessels in fundus photography. D) Assessment of E/P ratio, number of acellular vessels, and BRB breakdown by assays of retinal trypsin digestion and Evans blue respectively. E) Representative images of the of retinal vasculature by H&E-staining. White arrows point to acellular capillary. F) Representative figures of whole-mount retina stained with isolectin GS-IB4. G) Quantification of retinal microaneurysm, vascular density, and conjunctive vessels in whole-mount retina, analyzed by AngioTools. H) H&E staining of retinal histology sections. I) Quantification of retinal neurons in GCL layer, and thickness of IPL and INL. All data are indicated as mean \pm SD of five independent experiments. * $p < 0.05$, ** $p < 0.01$ and *** $p < 0.001$ versus Model group in STZ-induced Type I diabetic mice; # $p < 0.05$, ## $p < 0.01$ and ### $p < 0.001$ versus Control group in Type II diabetic Model (db/db mice).

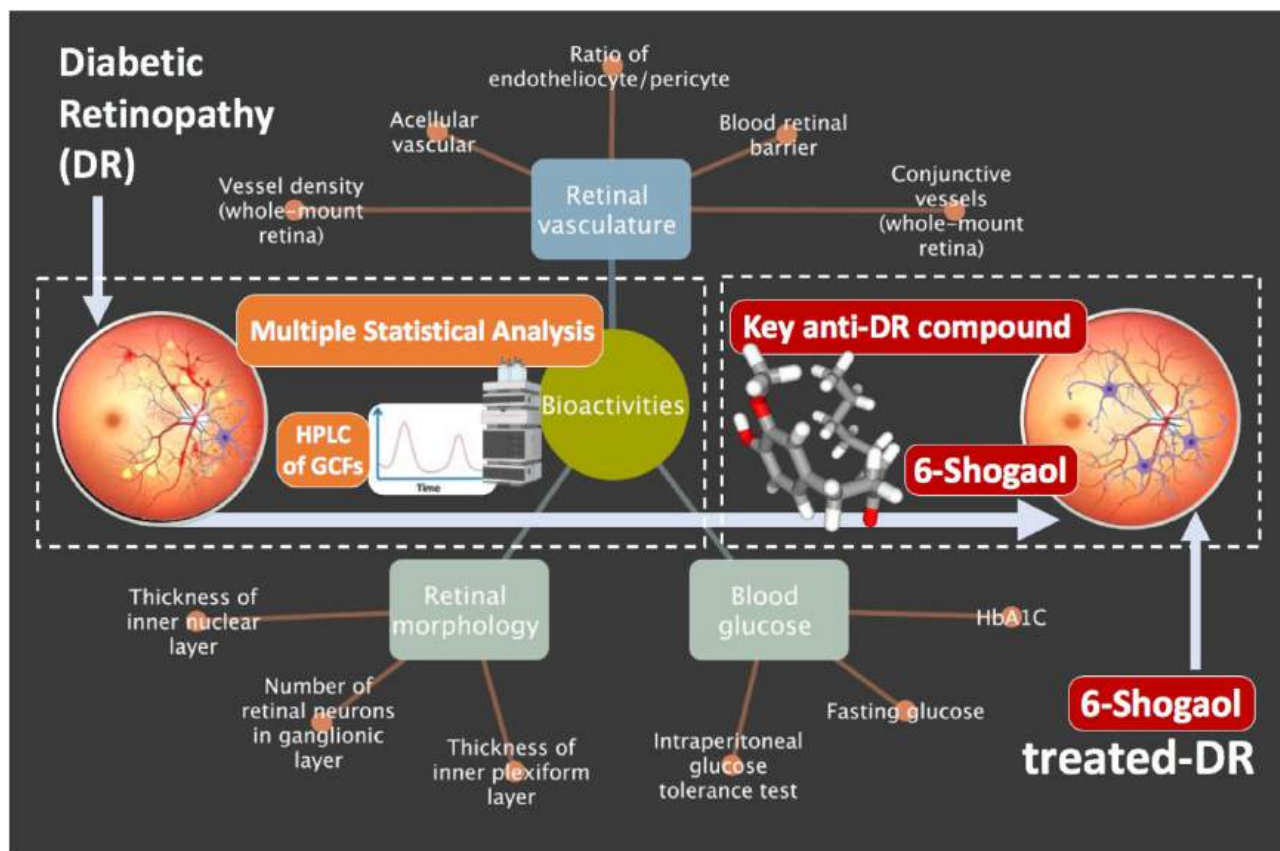


Figure 7. Schematic of mathematical prediction-bioactivity model underlying the inhibitory effect of 6-shogaol from GCF on the progression of diabetic retinopathy.

occurred in the analysis of GRA, MLRA, thus PCA is applied to curtail the multicollinearity with efficient interpretability.^[24] As a multivariate statistical method, PCA can combine the variables to mutually independent variables by directly mapping of high-dimensional data to a lower-dimensional space, which reflects the original information as much as possible. Herein, a combination of GRA, RBFA, MLRA in the model of Mathematical Prediction-Bioactivity offers scientific evidence for analyzing the relevance of chemical profiles and bioactive actions.

Based on the multivariate model prediction and experimental validation, both P12 (6-gingerol) and P13 (6-shogaol) were identified as the most weighed ingredients in DR treatment in both Type I (STZ induction) and leptin receptor-deficient Type II (db/db) diabetic mice. In addition, it is found that anti-DR property of 6-shogaol is superior to that of insulin, S4, and 6-gingerol in terms of treating vascular and neural complications in DR progression. Notably, the anti-hyperglycemia effects of 6-shogaol is much lower than that of insulin, suggesting that the anti-DR effect of 6-shogaol is in hypoglycemia-independent manner. 6-shogaol is reported to ameliorate the progression of diabetic nephropathy with its anti-inflammation and anti-oxidative activity.^[25,26] It is also demonstrated to attenuate retinal vasculopathy and neuropathy in our experiments. Of note, such a compound with holistic anti-DR efficacy is specifically seldom to observe. In general, one component is prone to have both synergistic and antagonistic actions in treating diseases. Several

possibilities as follows may explain this situation. First, according to the pairwise comparison analysis (Figure 5F), the 6-shogaol (P13) is negatively correlated with either 6-gingerol (P12) or a series of compounds mainly existed in coptis (especially the P5, P6, P7), suggesting that 6-shogaol-related negative correlation among compounds may strengthen the anti-DR action of GCF (e.g., in-vivo biotransformation among compounds). Meanwhile, it is documented that gingerol analogues can be thermally labile and undergo dehydration transform into shogaols in vivo,^[27] which is consistent with the result of pairwise comparison analysis (Figure 5F). Herein, gingerol was potentially converted to shogaol during the in vivo bioactivity transformation, of which shogaol was the most common dehydration product.^[28] These findings may elaborate why the difference of anti-DR effect between herbal combinations and 6-gingerol is not as conspicuous as that of 6-shogaol. Second, in a certain proportion of GCF, such as S4 (G:C = 1:1), particular substances mainly in coptis may enhance the conversion ratio of 6-gingerol to 6-shogaol in the GCF-treated diabetic mouse against DR.

In summary, 6-shogaol was verified as the predominant contributive compound in GCF for DR treatments in diabetic models. As a multivariate statistical approach, the Mathematical Prediction-Bioactivity model is feasible to evaluate the relevance between chemical profile and bioactivities of herbal medicine. These results allow us to establish a novel compound-mining strategy in a multicomponent system. Such a model is potentially

Table 2. Weight and ratio of ginger and coptis extract in GCF.

No.	Ginger [mg]	Coptis [mg]	Ginger:Coptis
S1	18.5	1.5	12.9:1
S2	15.7	4.3	3.6:1
S3	12.9	7.1	1.8:1
S4	10	10	1:1
S5	7.1	12.9	1:1.8
S6	4.3	15.7	1:3.6
S7	1.5	18.5	1:12.9

applicable not only in the field of medical treatment, but in the processes of pharmaceutical production, including drug quality control.

4. Experimental Section

Preparation of GCF by Uniform Design: Raw herbs of GCF were obtained from the Pharmacy of School of Chinese Medicine in the University of Hong Kong. For the preparation of GCF, all the herbs were weighted and thoroughly soaked in the water for 1 hour and then boiled twice (1 hour each time) with 10 times of distilled water (1:10 w/v). The remaining 1st-supernatant liquid was cooled in the room temperature and collected. Then, tenfold distilled water (1:10 w/v) was added to the drug residue and boiled twice followed by the collection of the 2nd-supernatant liquid. Afterward, the combination of 1st- and 2nd- supernatant liquid was concentrated and dried into the granulated powder by a freeze-dryer with vacuum pump at $-40\text{ }^{\circ}\text{C}$ for 5 days (ilShinBioBase, South Korea). All the power extraction was sterilized and stored in $-80\text{ }^{\circ}\text{C}$.

Uniform design (UD) is a space-filling technology whose application in medical experiments and industrial science is a novel endeavor. UD seeks variables that are equally scattered with high representativeness in the experimental domain.^[29] Also, UD accommodates the potential maximum number of levels for each experimental factor. Therefore, UD is capable of achieving the identical goal as other statistical design methodology like orthogonal design, along with fewer number of experiments. Based on the merits of the advanced technology, UD was applied for setting the number of levels and ratios of GCF by Data Processing System 7 and R with UniDOE package.

In addition, a UD-dependent second-order polynomial model was adopted to discover the minimum value the sum of squares of the residuals between the experimental and predicted values.

$$\gamma = \beta_0 + \sum_{i=1}^4 \beta_i x_i + \sum_{1 \leq i < j \leq 4} \beta_{ij} x_i x_j + e \quad (1)$$

Afterward, a UD-dependent matrix with uniformly designed ginger/coptis ratios in GCF was established. (Table 2).

Chromatographic Fingerprint Analysis: The fingerprints of GCF were gained by a C18 column (100 mm \times 2.1 mm id) (ACE, UK) in an Ultra Performance Liquid Chromatography (UPLC) system (Thermo Fisher Scientific, USA). Seven modifications of the ginger/coptis ratio in GCF were performed by uniform design prior to producing the fingerprinting plot according to a gradient elution procedure as described in Figure 3B. The mobile phase includes 100% acetonitrile and 0.085% H_3PO_4 respectively. The temperature of C18 column was maintained at $32\text{ }^{\circ}\text{C}$ with the 1 mL min^{-1} flow rate. Meanwhile, the selection of monitoring wavelength of ingredients in GCF was 288 nm. Additionally, as a method of unsupervised learning, k-means-based principal component analysis (PCA), clustering analysis (CA), and t-SNE (t-distributed stochastic neighbor embedding) analysis have been adopted for a dimensional reduction followed by iden-

tifying the differences in chemical components among the modified GCF, which is vector-quantified and visualized in R using FactoMineR, Factoextra, and Rtsne packages.

Factor Analysis: Factor analysis is a technique for condensing a mass of variables into similar patterns reflecting the major variation of the data source.^[30] 14 experimental observations for measuring the anti-DR effects of GCFs (S1–S7) were subjected to a PCA using a linear combination with varimax rotation by SPSS, which aims to produce the orthogonal factors and remain the discrepancy of data with a dimensional reduction. Those indices with SPSS-based Kaiser value larger than 1 were further proceeded in R with Factanal package to explain the clinical meaning. After the data reduction, new recombined independent factors (F1–F3) with sub-indicators (11 experimental indices) were accounted for 83.4% of the cumulative variance of all the variables. The higher the loading value is, the weight of the bioindicator in each factor is greater.

Gray Relational and Multiple Linear Regression Analysis: For gray relational analysis (GRA), GRA was adopted to identify the principal influential component in GCFs for the anti-DR action. Gray relational grade (GRG) is applied to rank the impact of comparison sequence, which is obtained by calculating the distance between the comparison and reference series without any hypothesis on the distribution pattern.^[31] The procedure was composed of 3 steps, including the establishment of gray relation, calculation of gray relational coefficient (GRC) and GRG. Briefly, all the data has undergone z-score normalization. GRC was preceded to calculated the GRG. The operational procedures in detail are implemented by the following Equations (1):

$$\begin{aligned} \Delta_{\min} &= \min_j \min_k |z_0(k) - z_j(k)| \\ \Delta_{\max} &= \max_j \max_k |z_0(k) - z_j(k)| \\ \Delta_{0j}(k) &= |z_0(k) - z_j(k)| \\ \gamma_j(k) &= \frac{\Delta_{\min} + \rho \Delta_{\max}}{\Delta_{0j}(k) + \rho \Delta_{\max}} \\ \gamma(z_0, z_j) &= \frac{1}{n} \sum_{k=1}^n \gamma(z_0(k), z_j(k)) \quad (j = 1, 2, \dots) \end{aligned} \quad (2)$$

Where the reference series $z_0(k)$ and comparative series $z_j(k)$ point to the 11 factors (F1–F11) and the peak areas of 13 compounds in GCFs (S1–S7), respectively. $\Delta_{0j}(k)$ is the deviation series of $z_0(k)$ and $z_j(k)$, while Δ_{\max} and Δ_{\min} is adopted to calculate the maximum and minimum deviations of $z_0(k)$ and $z_j(k)$. $\rho = 0.5$ (distinguish coefficient) is applied in this equation. The value of GRG (γ) was obtained by calculating the average GRC. The larger the value of GRG is, the higher of influential degree of the factor is. The processes of GRA were carried out by Grey Modeling Software 3.0.

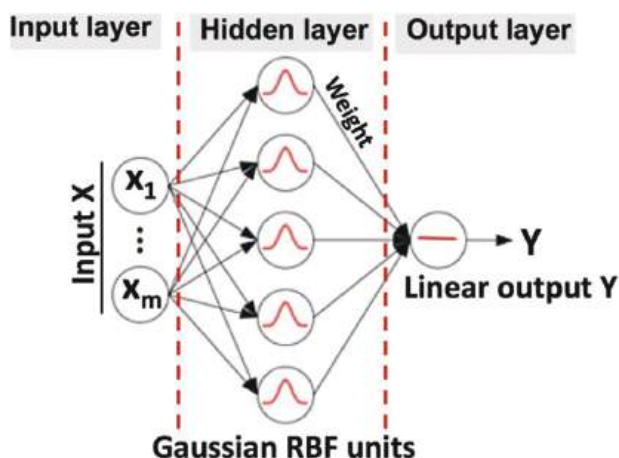
For multiple linear regression analysis (MLRA), the equations of MLRA were established between the factors F1 and F11 (dependent variable) and peak areas of 13 components (independent variable) in GCFs (S1–S7). The regression model was the following Equation (2):

$$\gamma = a_0 + a_1 x_1 + a_2 x_2 + \dots \quad (3)$$

where γ is the factor, and x is the peak areas of compound. Meanwhile, a_0 points to the regression constant, while a_1 and its onward are the regression coefficients. A regression equation was constructed when $p\text{-value} < 0.05$. The degrees of correlation between factors and compounds were evaluated by the value of regression coefficients. The larger the regression coefficient is, the higher the correlation degree is. The MLRA is processed by SPSS.

Support Vector Machine: Support vector machine (SVM) model can discriminate the classification of components via mapping the data vector to the high-dimensional feature space. Afterward, the hyperplane can be found followed by the differentiation of the classes with largest margin. Radial basis function (RBF) has been used in our study as the SVM-dependent machine learning. As a kernel function, RBF plays an important

role in the field of neural network.^[32] RBF maps the input samples to the high-dimensional descriptor space with weight determination, which may not be separated linearly. The training of the neural network includes clustering algorithm and weighting vectors. A probabilistic value representing for the independent variable importance of each factor will be given as an final output. The network of RBF is composed of three layers, including the input, hidden, and output layer as shown below,



In the RBF analysis of our study, the peak areas of 13 compounds were chosen as the input vectors for training the cluster centers and then projected to hidden layer as neuron units. After transformed by RBF, the values of the distance between the input vector and its center were determined by a series of training iterations. Each unit in the hidden layer was multiplied by its connected weight followed by feeding into the output layer, which then linearly generated the variable factors (F1–F11). Thus, the structure of RBF network between 13 peak areas and factors was established. The contributive degree of each compound was evaluated in accordance with the connection weight of variables. The RBF training progresses were performed by R using Nnet package.

Animal Study: All the animal experimental were undertaken after the approve of Committee on the Use Research (CULATR, ref: 4791-18) of the University of Hong Kong. C57/BL6N mice were purchased from the University of Hong Kong, while the C57BL/KsJ db/db (BKS.Cg-Dock7m +/+ Leprd/J) mouse exhibiting features of Type II diabetes were purchased from the Jackson Laboratory. Notably, the Type I diabetic mouse will be established by 5 consecutive injection of streptozotocin (STZ, 50 mg/kg/per i.p.). Those STZ-treated mice with fasting blood glucose ranging from 15 to 22 mmol L⁻¹ will recruit in our study as successful model of Type I diabetes. Animals were housed in places with pathogen-free food and water, along with a 12 hours light/dark schedule for 8 weeks. Mice were received insulin (2 U/kg/d) by intraperitoneal injection. Meanwhile, in terms of Table 2, mice were simultaneously treated with various ratios of herbs by gavage ($n = 5$ /group). Body weight were measured once a week. At the endpoint of each in vivo experiment, mice were sacrificed by pentobarbitone (200 mg/kg).

For the blood glucose measurement, fasting glucose were weekly performed. Intraperitoneal Glucose Tolerance Test (IPGTT) conducted at the end of experiment by the injection of glucose (2 g/kg b.w.). Glucose injection in IPGTT was prior to the assessment of blood glucose at the time-point 0, 30, 60, 90, and 120 min. In addition, the level of serum glycated Hemoglobin A1c (HbA1c) were tested by an ELISA kit (CLOUD-CLONE CORP, USA).

Blood–Retinal Barrier Permeability: Evans blue (Sigma, USA) quantitation technology was adopted to measure the permeability of blood–retinal barrier (BRB). The protocol was minor modified according to our previous publication. Briefly, at the end of in vivo study, mice were intravenously injected with Evans blue (45 mg/kg in 0.9% sodium chloride). After 3 h, mice were perfused by 0.1 M citrate buffer (PH = 3.5) followed by the retina

isolation. blood was centrifuged at 10 000 rpm for 20 min and 1/10 000 diluted with formamide (Sigma, USA). Retina was dried at 48 °C in a vacuum centrifugal concentrator (CentriVap, USA) followed by the centrifugation-based extraction of Evan blue dye in formamide for 100 min at 13 000 rpm. The concentration of Evans blue was determined under the absorbance of 620 nm. The quantification of the permeability of BRB was performed by the equation below,

$$\frac{\text{Retinal EB } (\mu\text{g}) / \text{Retinal dry weight} (\text{mg})}{\text{Plasma EB concentration } (\mu\text{g} / (\mu\text{L}) \times \text{Circulation time} (\text{h}))} \quad (4)$$

Retinal Histology: For the study of retinal structure, the retina was collected from eyeballs followed by incubating with 4% paraformaldehyde for 6 h. Then, fixed retina was immersed in the ethanol for gradient dehydration (70%, 80%, 90%, 95%, and 100% ethanol) once an hour. Afterward, retina was embedded in the paraffin and cut into section (5 μm thick) followed by the rehydration with graded ethanol (70%, 90%, 100%). Subsequently, retina slides were stained with hematoxylin and eosin (H&E) dye for histological study, including the quantitation of neurons (retinal ganglion cell and amacrine cell) in retinal ganglion cell layer, the thickness of inner plexiform layer and inner nuclear layer. All these measurements were calculated by ImageJ (NIH, USA). Images were gained by the light microscope (Olympus BX43, Japan).

Measurement of Retinal Vasculature: Retinal Fundus Photography in Living Mice: For the measurement of retinal angiogenesis in the living animal, ocular fundus was captured by an ophthalmoscope-dependent system (a 78D ophthalmoscope with a smart phone, and the application of Filmic Pro). It is a direct and non-contact approach for fundus photography. Particularly, the whole process should be implemented in a dark environment. Briefly, the 78D lens was vertically placed above the cornea. By adjusting the coaxial light from the camera, a clear visual field will be acquired by Filmic Pro. The quantification of vascular networks with morphological and spatial parameters has been carried out by AngioTool (NIH, USA), including the detection of cotton-wool spots, vascular density, and conjunctive vessels in retinal fundus.

Trypsin-Based Isolation of Retinal Vasculature: For the observation of retinal vasculature by trypsin digestion, fixed retinal was incubated with 3% trypsin (Amresco 1:250) in 0.1 M Tris buffer (pH = 8.2) and gently shaking for 3 h at room temperature. Afterward, the digested surface tissues were washed away by PBS followed by H&E staining. Then, the retinal vessels including adherent endothelialocytes, pericytes and acellular capillaries were visible and quantified in 8 random fields. The figures were captured by a light microscope (Olympus BX43, Japan).

Vasculature Immunofluorescence in Whole Mount Retina: Flat-mounted retina was fixed in 4% paraformaldehyde for 2 h and post-permeabilized in 70% ethanol for 1 h. Then, retina was incubated in 1% Triton X-100 (Sigma, USA) for 1 h followed by blocking in the mixture of 10% goat serum and 0.3% Triton X-100 for 2 h. Afterward, retina was immunostained with Alexa Fluor-488-conjugated isolectin GS-IB4 (0.02 mg mL⁻¹, Invitrogen, CA) for 24 h. After the final washing by PBS, retina was placed by RGC layer up. AngioTool was applied to measure the vascular density and conjunctive vessel in whole mount retina ($n = 5$ /group). ImageJ was adopted for the quantification of retinal microaneurysm. All images were obtained using a confocal laser scanning microscope (200× magnification, Carl Zeiss LSM 780, USA).

Statistical Analysis: All the animals were grouped by randomization ($n = 5$ /group). For the comparison between groups, *t*-test was applied for data with normal distribution. Meanwhile Mann-Whitney U test was used for data with skewed distribution. Furthermore, for the comparisons of more than two groups, both one-way ANOVA and Kruskal-Wallis test were used. All the data were shown as mean ± SD. A value of $p < 0.05$ was considered as a significant difference.

Supporting Information

Supporting Information is available from the Wiley Online Library or from the author.

Acknowledgements

The authors would like to express thanks to Mr Keith Wong, Ms Cindy Lee, Mr Alex Shek and the Faculty Core Facility for their technical support. This research study was supported by Research Grant Council, HKSAR (Project Code RGC GRF 17152116), Commissioner for Innovation Technology, HKSAR (Project Code ITS/091/16FX) and Health and Medical Research Fund (Project Codes 15162961 and 16172751). Wong's donation (project code: 200006276), and a donation from the Gaia Family Trust of New Zealand (project code: 200007008).

Author Contributions

Y.F. and N.W. conceived and designed the study; C. Z. and N.W. did the experiments. C. Z., N.W., Y. X., H.Y.T., and Y. F. wrote the manuscript. C. Z., N. W., and Y.F. interpreted the data. All authors discussed and revised the manuscript and approved the final manuscript.

Conflict of Interest

The authors declare no conflict of interest.

Data Availability Statement

The data that support the findings of this study are available from the corresponding author upon reasonable request.

Keywords

diabetic retinopathy, medical sciences, pattern recognition, target identification

Received: November 5, 2020

Revised: January 8, 2021

Published online: May 4, 2021

- [1] W. Zheng, J. Wu, J. Gu, H. Weng, J. Wang, T. Wang, X. Liang, L. Cao, *Front Pharmacol* **2020**, *11*, 147.
- [2] N. Wang, H. Y. Tan, S. Li, D. Wang, Y. Xu, C. Zhang, W. Xia, C. M. Che, Y. Feng, *Sci. Adv.* **2019**, *5*, eaav0198.
- [3] T. Y. Tang, F. Z. Li, J. Afseth, *Chin. J. Integr. Med.* **2014**, *20*, 883.
- [4] Q. Ye, R. Zhou, M. A. Anwar, A. N. Siddiquei, F. Asmi, *Int J Environ Res Public Health* **2020**, *17*, 1355.
- [5] X. Hu, D. Wang, Y. Pang, Z. Wu, H. Huan, Z. Chen, W. Li, *J Tradit Chin Med* **2020**, *40*, 73.

- [6] J. J. Steinle, *Mol Vis* **2020**, *26*, 355.
- [7] R. Cheloni, S. A. Gandolfi, C. Signorelli, A. Odone, *BMJ Open* **2019**, *9*, e022188.
- [8] R. Appanraj, H. Duraiswamy, V. Saravanan, G. Manayath, N. Venkatesh, *Indian J. Ophthalmol.* **2020**, *68*, 1201.
- [9] B. Pang, Q. W. Li, Y. L. Qin, G. T. Dong, S. Feng, J. Wang, X. L. Tong, Q. Ni, *Medicine* **2020**, *99*, e19102.
- [10] J. M. Yang, G. Li, M. Wang, Y. X. Jin, F. J. Zheng, Y. Sun, Y. S. Gao, S. J. Zhang, P. F. Kang, L. Chen, M. Y. Wu, S. Y. Xu, Y. H. Li, *J. Evidence-Based Complementary Altern. Med.* **2017**, *2017*, 7250340.
- [11] N. Khandouzi, F. Shidfar, A. Rajab, T. Rahideh, P. Hosseini, M. M. Taheri, *Iran J Pharm Res* **2015**, *14*, 131.
- [12] T. Arablou, N. Aryaeian, M. Valizadeh, F. Sharifi, A. Hosseini, M. Djalali, *Int J Food Sci Nutr* **2014**, *65*, 515.
- [13] J. C. Li, X. F. Shen, J. A. Shao, M. M. Tao, J. Gu, J. Li, N. Huang, *Drug Des Devel Ther.* **2018**, *12*, 2695.
- [14] Z. Zhen, B. Chang, M. Li, F. M. Lian, L. Chen, L. Dong, J. Wang, B. Yu, W. K. Liu, X. Y. Li, P. J. Qin, J. H. Zhang, X. L. Tong, *Am J Chin Med* **2011**, *39*, 53.
- [15] X. Zhang, *Open Biomed Eng J* **2015**, *9*, 266.
- [16] Z. A. Raza, N. Ahmad, S. Kamal, *Biotechnol Rep* **2014**, *3*, 86.
- [17] W. W. Y. Ng, S. Xu, T. Wang, S. Zhang, C. Nugent, *Sensors* **2020**, *20*, 1479.
- [18] Y. Cho, O. Hieda, K. Wakimasu, K. Yamamura, T. Yamasaki, Y. Nakamura, C. Sotozono, S. Kinoshita, *Am. J. Ophthalmol.* **2019**, *207*, 326.
- [19] M. Schenone, V. Dancik, B. K. Wagner, P. A. Clemons, *Nat. Chem. Biol.* **2013**, *9*, 232.
- [20] S. K. Musani, D. Shriner, N. Liu, R. Feng, C. S. Coffey, N. Yi, H. K. Tiwari, D. B. Allison, *Hum Hered* **2007**, *63*, 67.
- [21] W. Peng, J. Zhong, J. Yang, Y. Ren, T. Xu, S. Xiao, J. Zhou, H. Tan, *Microb. Cell Fact.* **2014**, *13*, 54.
- [22] N. Conaway, K. J. Kurtz, *Neural Comput* **2017**, *29*, 861.
- [23] S. Anita, P. A. Priya, *Curr. Med. Imaging Rev.* **2019**, *15*, 461.
- [24] K. P. Vatcheva, M. Lee, J. B. McCormick, M. H. Rahbar, *Epidemiology* **2016**, *6*, 227.
- [25] Y. Xu, L. Bai, X. Chen, Y. Li, Y. Qin, X. Meng, Q. Zhang, *Biomed. Pharmacother.* **2018**, *97*, 633.
- [26] J. Y. Na, K. Song, J. W. Lee, S. Kim, J. Kwon, *Eur. J. Pharmacol.* **2016**, *788*, 241.
- [27] R. B. Semwal, D. K. Semwal, S. Combrinck, A. M. Viljoen, *Phytochemistry* **2015**, *117*, 554.
- [28] S. Bhattarai, V. H. Tran, C. C. Duke, *J. Pharm. Sci.* **2001**, *90*, 1658.
- [29] J. Zhang, L. Tang, B. Liao, X. Zhu, F. X. Wu, *Biomed Res. Int.* **2019**, *2019*, 4979582.
- [30] S. Y. Wei, H. Y. Zhang, Y. T. Yin, L. J. Ma, L. Li, Y. M. Dong, Y. Fan, *Dermatol. Ther.* **2020**, *33*, e13690.
- [31] P. Yao, K. Zhou, H. Lin, Z. Xu, S. Yue, *Materials* **2019**, *12*, 3662.
- [32] H. Lin, Q. Dai, L. Zheng, H. Hong, W. Deng, F. Wu, *Chemosphere* **2020**, *248*, 125999.